POLITECNICO DI TORINO
Repository ISTITUZIONALE

Cost-effective Line Termination Net for IGBT PWM VSI AC Motor drives

(Article begins on next page)

20 April 2024

Cost-effective Line Termination Net for IGBT PWM VSI AC Motor drives

A. Fratta (member), G.M. Pellegrino, F. Scapino (member) and F. Villata (member)

Dept. of Electrical Engineering, Politecnico di Torino, C.so Duca degli Abruzzi, 24, 10129 Torino ITALY

Abstract - **Full performance of series Line Termination Net has been already achieved by means of parallel ferrite-core inductors and not inductive power resistors, affecting integration and cost-effectiveness in medium-power PWM AC motor drives. A novel LTN design concept is here presented, namely IRONET, based on the exploitation of the inductor core loss as part of the wanted high-frequency LTN response. Iron cores are adopted instead of larger ferrite-core thanks to proper eddy-current density, set by design of lamination thickness and winding turns. The effective high-frequency behaviour of lossy power inductors is analysed and discussed, defining small-size R-C simple compensation. An IRONET prototype has been realised and tested for a 55kW-rated IGBT IM, showing IRONET effectiveness very close to full performance even by common .35mm laminations.**

I. Introduction

In the field of PWM VSI drives, the reliability of AC motors is increasingly related to the transmission of fast IGBT commutation edges [9].

Several Line Termination Net (LTN) concepts have been proposed at both power transmission line ends [1,5,6,7,8], in order to avoid dangerous AC motor windings voltage derivative and peak values as well as to reduce current spikes and overall drive EMI.

The solution here considered is based on the "series" LTN disposed at near-end, inverter side as in Fig. 1, of the power transmission line. This solution has been defined as the best balance among different design goals and operating performances [1], showing satisfactory cost-effectiveness in the low power range, being able to cancel motor overvoltage related to long power cable as well as to drastically reduce current spikes ringing and EMI.

In medium to high power drives this series LTN concept provides full performance as well, however LTN devices size is hardly increasing with power [3,4]: for a 55kW rated I.M., bulky 90µH, 110Arms ferrite-core inductors and 25W not-inductive power resistors would be needed.

II. Summary on Series LTN Design Items.

Referring to the simplest solution for the series LTN consisting of three parallel connected resistor-inductor circuits, shown in Fig. 1, effective design criteria have been given and tested in previous works [1,2,3].

A. LTN resistance design.

In a three-wire near-end series termination, it is convenient to equate the LTN resistance "R" to a particular value "Z_{OW}" (1), ensuring the best attenuation of power line reflected waves, as related to contemporary common and differential modes generated by 3ϕ PWM VSI IGBTs:

$$R = Z_{0W} = \frac{Z_{0c} - Z_{0d}}{6} \cdot \left[\sqrt{1 + Z_{0c} Z_{0d} \left(\frac{6}{Z_{0c} - Z_{0d}} \right)^2} - 1 \right] \quad (1)$$

where "Z_{0c}" and "Z_{0d}" represent the cable characteristic impedances, defining the line propagation properties of common-mode (zero-sequence) and differential-mode (3ϕ-symmetrical) electrical variables, respectively.

B. LTN inductor sizing criteria.

The LTN inductance "L" is connected in parallel to the resistor to reduce LTN power loss related to power flow. However, we must observe that the system exhibits a main differential-mode resonant frequency, due to the overall LTN+cable+motor inductance and capacitance, in the order of hundred kHz (250 kHz for our reference system).

This main resonance must be dumped to control the residual overshoot on motor voltage response. The critical damping is then adopted as main criterion for L sizing:

$$\alpha_L \cdot L \geq 2 \cdot C_D \cdot (R \cdot \alpha_R)^2 \quad (2)$$

where "C_D" accounts for all line-to-line effects, affecting the propagation of differential mode, and the coefficients:

$$\alpha_L = \frac{1}{1 + L/L_S}; \; \alpha_R = \frac{1}{1 + R/R_S} \quad (3)$$

are partition coefficients, being "L_s" mainly related to the motor leakage inductance and "R_s" to load damping effects (mainly motor iron losses).

C. LTN power terms.

Two main terms can summarise LTN total power loss.

$$P_{LTN} = P_I + P_{HF} \quad (4)$$

"P_I" accounts for LTN voltage drops related to the conduction of the fundamental component (at electrical pulsation) of line currents:

$$P_I \equiv 3 \cdot \left(\omega_{el} \cdot L \cdot I_{line} \right)^2 \frac{1}{R} + 3 \cdot R_{Cu} \cdot I_{line}^2 \quad (5)$$

P_I is not considered in this work: the first term is related to high-frequency LTN design, however it is negligible with respect to others here considered (6); the second term represents the copper loss due to current flow in the winding series resistance, which is dominating the power inductor design together with iron losses, while not related to LTN high-frequency behaviour specifications.

Two "high frequency" terms are evaluated for design:

$$P_{HF} = P_{PWM} + P_{SW} \quad (6)$$

P_{PWM} refers to PWM ripple voltage drop on the LTN, depending both on DC-BUS voltage and on the amplitude of the modulation index (actual fundamental AC voltage); calculation of its maximum value [3] yields:

$$P_{PWM} \leq 2 \cdot \left(\frac{1}{\pi} \frac{V_{BUS}}{1 + L_S / L} \right)^2 \frac{1}{R_{PWM}} \quad (7)$$
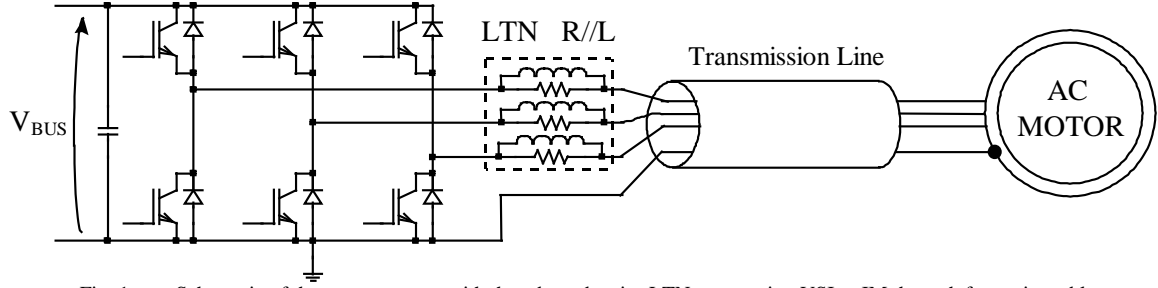
Fig. 1. Schematic of the power system with the adopted series LTN, connecting VSI to IM through four-wire cable.

where the LTN resistance value "R_{PWM}" is specifically evaluated around twice the switching frequency as the dominant one among the PWM harmonics generated by the VSI; note these ones are reduced on the LTN as a function of the inductive partition ratio (3).

At last, "P_{SW}" accounts for the minimisation of cable reflections and for the LTN contribution in damping the oscillating voltage response to each VSI step. Every VSI step, charging and discharging at the same time common- and differential-mode capacitances, implies two related damping terms analytically complex while scarcely affected by LTN inductor behaviour [4].

D. 55 kW reference case.

A 55kW-rated IM drive, fed by a VSI by means of a 14m-long power cable according to Fig.1, gives the figures summarised in Table I, with reference to the high frequency terms (6) of the maximum power lost by constant terminating resistors in the case of 90μH ferrite-core inductors (assumed to have negligible losses).

Worst-case working conditions	P_{SW}	P_{PWM}	P_{HF}
V$_{BUS}$=600V; V$_{AC}$=270Vrms line-to-line (PWM index =0.7351)	22.3 W	24 W	46.3 W

TABLE I. MAXIMUM POWER LOST BY CONSTANT-VALUE LTN RESISTORS. (R=64Ω, L= 90μH FERRITE-CORE INDUCTORS, 14M-LONG CABLE).

Looking at the numerical values, it comes into evidence why the simple LTN implementation, with a resistor-inductor parallel, is not suitable in the medium to high power range, because it would be too expensive and encumbered requiring big size ferrite-core inductors and not-inductive power resistors.

III. IRONET Cost-effective Power LTN.

A novel design concept is proposed to obtain a low-cost implementation of the series LTN suitable for medium-to-high power IGBT PWM motor drives.

The basic concept relies on size and cost reduction of the power inductors by using iron instead of ferrite cores.

Accurate design of iron quality and lamination thickness could achieve proper iron loss density, thus avoiding further power resistors for LTN realisation, by exploiting the iron-core losses in the LTN design as part of wanted LTN damping effects.

To approach the IRONET design, some considerations must be taken into account about the power inductor:
a) the "stray" leakage inductance impedes the direct "access" to eddy currents;
b) "apparent" core inductance and resistance are depending on frequency according to frequency-dependant distribution of eddy currents inside the iron-core.

A. Reference lumped-parameter model.

The simplest equivalent circuit in Fig. 2 of is adopted as reference for power inductors, giving evidenced to iron-core and stray flux linkages by means of the coupling coefficient "k". The resistance "R_{CORE}" accounts for iron-core losses effect and it is here considered a constant value.

The wanted LTN behaviour (parallel R–L as in Fig.1) is equivalently obtained, overcoming the leakage inductance effect by simple R-C compensation design relationships:

$$R_{CORE} = R \cdot k^2 \tag{8}$$

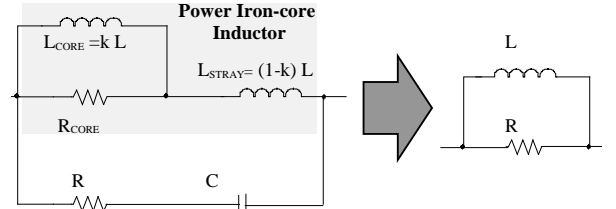$$C = \frac{L}{R^2} \cdot \frac{1-k}{k} \tag{9}$$

Fig. 2. Reference lumped-parameters model for power inductor and R C high-frequency compensation adopted for IRONET inductors.

B. Laminated iron-core frequency response.

The flux density distortion along laminations width due to eddy currents distribution takes to well known apparent L_{core} and R_{core} frequency responses [10,11].
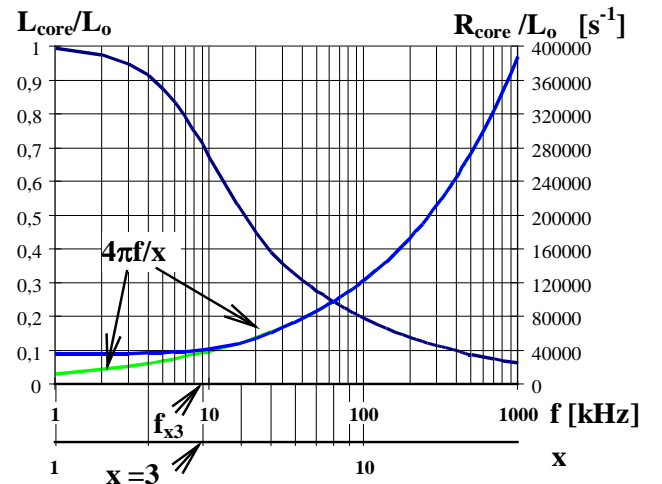

Fig. 3. Calculated laminated iron-core parameters behaviour due to eddy currents (hysteresis neglected). Absolute frequency scale for the adopted oriented-grain iron core laminations: thickness d=0.35 mm.

These ones are reported in Fig.3, with reference to the "dc-inductance" "L_o", according to (10):

$$\frac{R_{core}}{L_o} = \frac{4\pi f}{x} \frac{sinh^2(x) + sin^2(x)}{[\cosh(x) + \cos(x)] \cdot [sinh(x) - sin(x)]} \tag{10}$$

where the per-unit variable "x" is :

$$x = d\sqrt{\pi \cdot \mu\sigma \cdot f} \qquad (11)$$

given by the iron properties, magnetic permeability "μ" and conductivity "σ", and the lamination thickness "d".

In Fig.3 evidence is also given to a peculiar "cross-over" frequency "f_{x3}", found for $x=3$:

$$f_{x3} = \frac{9}{\pi \cdot \mu\sigma \cdot d^2} \qquad (12)$$

calculated as the intersection of low-frequency value:

$$\frac{(R_{core})_{DC}}{L_o} = \frac{12}{\mu\sigma \cdot d^2} \qquad ; \quad f \ll fx3 \qquad (13)$$

with the simplified high-frequency model:

$$\frac{R_{core}}{L_o} \rightarrow 4\pi \frac{f}{x} \qquad ; \quad f \gg fx3 \qquad (14)$$

Generally speaking, it would be useful to set the PWM frequency $\ll f_{x3}$, in order to get minimum the effects of frequency-depending parameters.

C. IRONET design items.

Unfortunately, the desirable LTN impedance behavior with frequency is the opposite of what obtainable according to analytical results reported in Fig. 3:
1) at PWM frequency and main harmonics, PWM losses (7) can be reduced by decreasing the parallel core inductance and by increasing the resistance $(R_{core})_{PWM}$;
2) at main (first) resonance frequency (250kHz in the case) the LTN inductance should be as high as possible to reduce current peaks and to increase resistance damping effect (2), the losses being set by overall (line + motor) parasitic stored charge variations at each PWM step;
3) at line reflection frequency (5 MHz in the case) the LTN resistance is suitably set by not-inductive resistors, as in Fig. 2, however the high-frequency inductor behavior should hold low resistance to allow for small-power resistors by small compensating capacitance value.

On the other hand, IRONET concept would allow for full exploitation of iron core flux density, up to saturation corresponding to peak value of fundamental load current.

The conclusion is that core material and lamination thickness must be suitably chosen to:
a) set the winding turn-number (square) to achieve the wanted inductor resistance at PWM frequency;
b) set the core cross-section area for full flux density;
c) reduce as much as possible the core resistance sweep from PWM up to the first natural system resonance frequency (laminations as thin as possible).

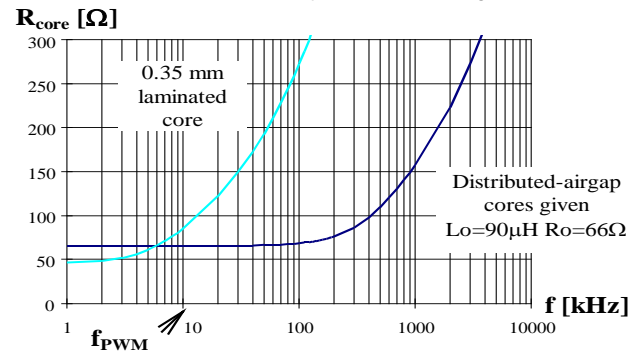### D. IRONET improvement by distributed-airgap cores.

R$_{core}$ [Ω]

Fig. 4.   Rcore calculated frequency responses of laminated cores.

Better IRONET inductor frequency responses could be achieved by distributed instead of concentrated airgap. This is true according to (12) if the reluctance distribution can be accounted as a reduced value of the homogeneous permeability μ of the laminated ferromagnetic material.

A sample of possible frequency response improvements is reported in Fig. 4, where the adopted laminated-core inductor (0.35 mm, concentrated airgap) is compared with a theoretical family of laminated cores designed for given apparent time constant ($90\mu H/66\Omega$). This is achieved by constant $\mu\sigma d^2$ value according to (12), that is by low values of relative permeability (one possible design example is $\mu_{rel}=10$, $\sigma=1/46\cdot10^8$ $[\Omega m]^{-1}$, $d=0.74mm$).

IV. IRONET Prototype Validation.

A. Laminated-core inductor prototype.

An IRONET inductor prototype has been designed for the reference 55kW PWM IM drive supplied through a 14m-long cable. The specifications are reported in Table II on the basis of wanted "constant" parallel resistance behaviour, set to $Z_{0w}=66\Omega$ (1) also at PWM frequency, thus keeping the PWM LTN loss very close to Table I design value ($\cong24W$ 3Φ) [3].

R$_{core}$ @10kHz (5.5kHz PWM)	$(R_{core})_{PWM} \cong 66$ Ω
Low frequency LTN inductance	L = 90uH
Rated IM peak current	$I_{peak} = 150$ A
Maximum dc-link voltage	$V_{BUS}=600V$

TABLE II. IRONET INDUCTOR SPECIFICATIONS.

A standard twin "U" 0.35mm-laminated oriented-grain wounded iron core has been chosen. According to experimental tests on the core resistivity, (R$_{core}$)$_{PWM}$ value have been set by proper turns number "N". The airgap thickness Δ_{airgap} is due to considerable fringing effect.

Core length	$l_e = 0.19m$
Cross-section area	$A_e = 3.2cm^2$
Peak flux density	$B_{peak} =1.76$ T (@150A)
Turns number	N=24 (12 per column)
Airgap thickness	$\Delta_{airgap}=3mm$ (1.5mm x2)

TABLE III. PROTOTYPE INDUCTOR CHARARACTERISTICS.

B. Measurements and frequency response compensation.

The frequency response of the inductor prototype has been firstly measured by means of a vector impedance meter, that is by very small mmf excitation. The results are reported in Fig. 5 in terms of equivalent parallel core inductance and resistance.

For better iron-core parameters evaluation, estimated series stray inductance (3μH) and test winding resistance (7mΩ) have been subtracted from measured impedance.

These small-signal measurements should be considered valid ones only within the tenth kHz to few MHz range, since a resonant frequency is reached around 15MHz, while at lower frequency the magnetic hysteresis becomes dominating the parallel resistance value.

For deeper evaluation of hysteretical effects, single points of parallel equivalent core resistance are reported in Fig. 5, as evaluated for sinusoidal 50mT and 0.5T peak excitation. These ones show resistance values depending on amplitude at low frequency, while converging to small-signal measurements in the PWM frequency range.
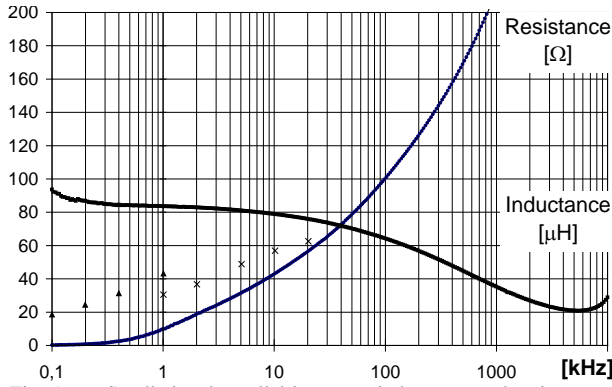
Fig. 5. Small-signal parallel iron-core inductance and resistance vs. frequency; equivalent core resistance points at 50mT (**X**) and 0.5T (**Δ**) excitation.

The inductor high-frequency behaviour is compensated according to Fig. 2 concept and scheme, while by design criteria not directly related to simple ones (8,9), since the large increase of core resistance has mostly to be compensated instead of stray inductance effect.

Fig. 6 reports the measured parallel real and imaginary parts of the complete IRONET, adopting the chosen compensating circuit $C=6nF$, $R=66\Omega$. The compensation inaccuracy is purposely displaced in the sense of reducing as much as possible the R-C time constant, thus minimising the power size of the extra resistor.
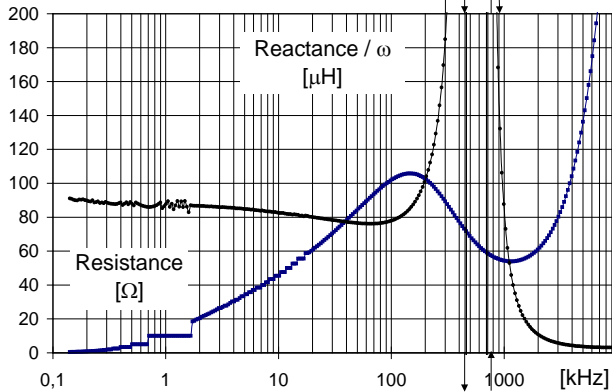

Fig. 6. Total IRONET parallel resistance and reactance/ω with R-C compensation: 0.35mm laminated prototype inductor; R=66 Ω, C=6nF.

C. IRONET model and power system simulation.

The adopted compensating circuit is evaluated with the aid of a lumped-parameters model of the IRONET inductor, derived from the experimental measurements reported in Fig. 5. These ones have been fitted with reference to the simple model shown in Fig. 7, suited for simple interpolation of distributed and concentrated parameters. To determine the model parameters, the fitting criterion over the frequency range covered by PWM harmonics has been adopted, leading to Fig. 7 graphs.

Even though at high-frequency the response is dominated by a very small leakage inductance (3µH), in the medium-frequency range, where power losses concentrate, the model gives evidence to a behaviour which can be considered equivalent to a smaller effective coupling coefficient. In this sense the compensating capacitance value around 6nF can follow also by properly adapting the design relationship (9). For higher-frequency matching to line reflections, the LTN extra resistor value is held equal to $Z_{0W}=66\Omega$ (1).
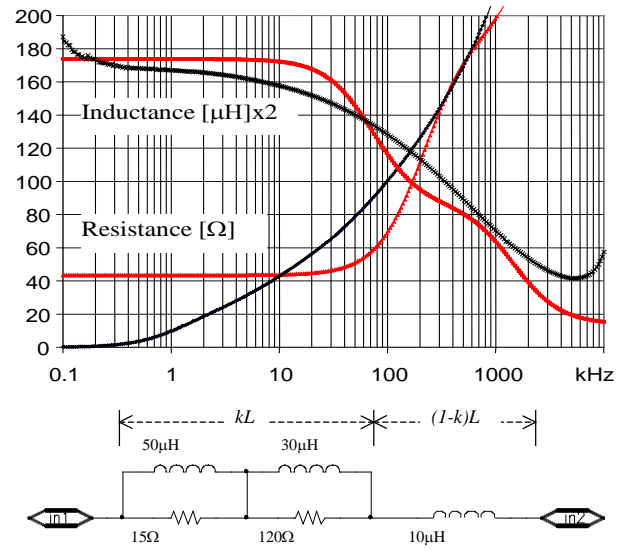

Fig. 7. Inductor core model response compared with Fig.5: 3µH series inductance subtracted from the reported lumped-parameters model.

The resulting power rating of the extra not-inductive resistor is bigger than would be expected by adopting an iron-core performing higher effective coupling coefficient.

The iron-core inductor model is here used for numerical Spice simulation tests of the compensated IRONET circuit in the complete drive system, verifying the extra resistor power sizing by estimating the power loss share.

The power system is modelled according to well experienced Spice circuit [2], reported in Fig. 8, excited by an input voltage pattern that gives rise to a modulation index close to the worst-case IM drive operation, from the PWM losses point of view (Table I) [3].

The power cable is modelled by the distributed parameters equivalent circuit depicted in Fig. 8, composed by three decoupled transmission lines and needed input-output transformations of three-phase variables into the three fundamental "α,β,o" components, the first two for differential (symmetrical components) and the last one for common (null sequence) propagation modes.

The high-frequency motor model reported in Fig. 8 is as accurate as possible by lumped parameters, accounting for every physical effect which can be consistently measured: "L_m" represents the leakage inductance; "R_m" models motor iron losses; "C_g , C_w" are the parasitic capacitance values accounting for winding-end to ground and winding-to-winding coupling effects, respectively; inner e.m.f. generators "E_j" account for rotation of magnetising flux.

The resulting PSpice simulations perform a very satisfactory match with the experimental results, like the motor voltage responses reported in Fig.9, showing equivalent overshoot amplitude and damping effect.

The IRONET losses can be then reliably verified, reported in Fig. 9 as the rise of lost energy within the selected single PWM period. Its PWM pattern effects on P_{HF} (6) are closely representative of worst-case drive operating condition in the complete electrical period.

The resulting average power loss is $P_{HF}=49.8W$, being composed of $P_{CORE}=39.0W$, lost in the three iron-cores, and of $P_R=10.8W$ lost in the extra not-inductive resistors.

Hence, the prototype implementation of the IRONET inductor by available common core material is satisfactory, since three cheap 5W-rated resistors and small 5.6nF capacitors are requested for its complete compensation.
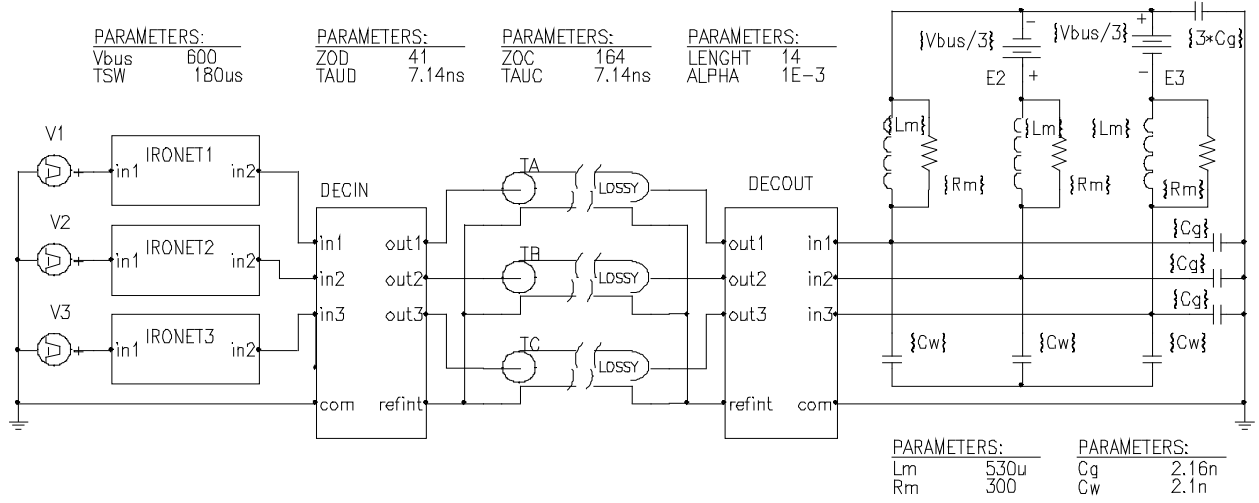
Fig. 8.   Power system schematic adopted for Spice simulation of the IRONET design; IRONET inductor prototype model according to Fig.7, with R=66W and C=6nF compensation; motor model as reported; four-wire 14m-long power cable modelled by reported lossy-line propagation parameters.
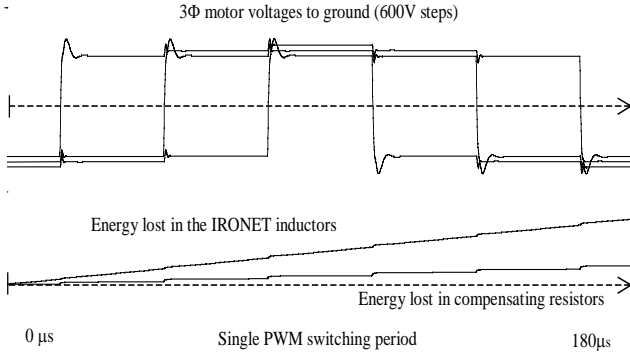

Fig. 9.   PSpice simulation of IM voltages to ground and energy lost by IRONET devices; PWM pattern representative of IM drive worst-case.

V. Experimental results.

A commercial IGBT PWM Induction Motor, 400V 55kW-rated energy-saving type, drive has been equipped with the proposed IRONET inserted at inverter-side of 14m-long commercial three-phase+ground power cable. The IGBT PWM VSI is supplied at 380V so that the dc-bus voltage is close to 500V.

The high-frequency behavior has been "corrected" by two small film capacitors (220nF), connected from dc-bus rails to power ground. Equivalently to the grounded negative-rail in Fig. 1, these capacitors would stabilize the high-frequency behavior of the IGBT inverter, otherwise it should be depending on diode bridge operation and on actual mains impedance. However, at lower frequency these two capacitors still allow for floating dc-link.

Figures from 10 to 11 report line voltage, with respect to wanted reference potentials, and homologous line current responses to an IGBT turn-on commutation, where the switched current is around 20A. Figs. 10 and 11 refer to responses without any LTN. Fig. 10 reports the far-end line motor voltage measured with respect to star common-tap, while Fig. 11 reports the same motor terminal potential with respect to ground. The dangerous doubling spike on the phase winding in Fig. 10 is not directly seen at motor terminals, that is with respect to motor ground as in Fig.11. The line current response is not dangerous for IGBT reliability (tenth A), while representative of generated EMI due to high frequency oscillating response.

Comparable with the previous ones, Figs. 12 and 13 are kept after insertion of the proposed prototype (complete IRONET concept). The voltage responses are both considerably better than without IRONET, with small residual overshoot and good damping. The reduction of EMI is appreciated on the current response, with reduced peak current and no ringing. In the same operating conditions, Fig. 14 reports the inverter-side line response.

At last, Figs. 15 and 16 report the responses at both line ends by inserting only the IRONET inductance without R-C high-frequency compensation. The result is intermediate on voltage overshoot, while still satisfactory on the reduction of current peaks and motor voltage derivative.
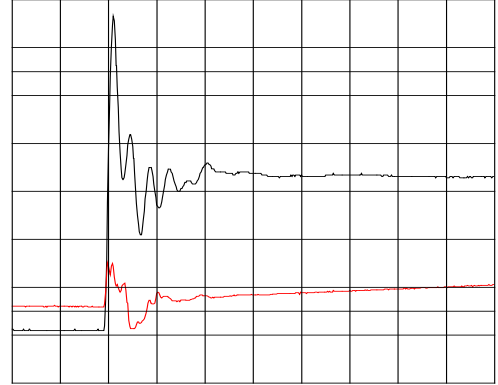

Fig. 10.   Motor voltage to star-common-tap [100V /div.] and line current [10A /div.] time responses [2μs /div.] without any LTN.
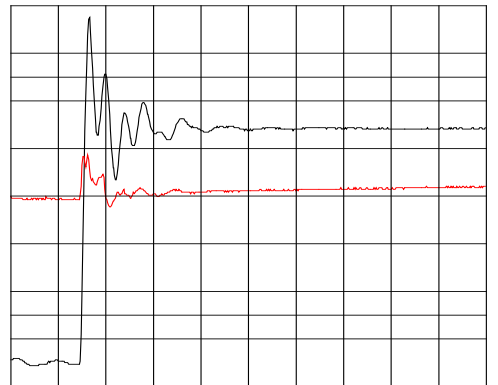

Fig. 11.   Motor voltage to ground [100V/div.] and line current [10A/div.] time responses [2μs /div.] without any LTN.
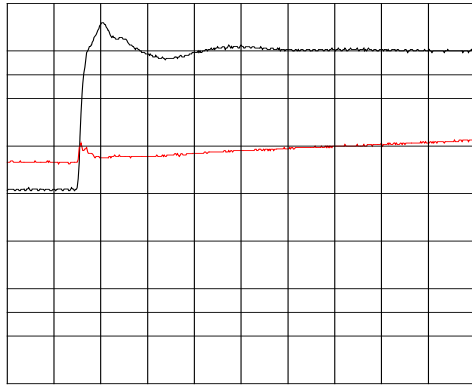
Fig. 12.   Motor voltage to star-common-tap [100V/div.] and line current [10A/div.] time responses [2μs /div.] with complete IRONET.
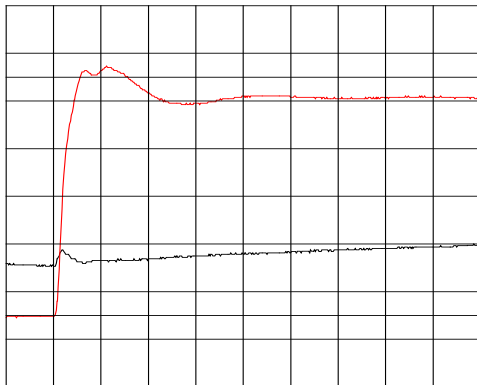

Fig. 13.   Motor voltage to ground [100V/div.] and line current [10A/div.] time responses [2μs /div.] with complete IRONET.
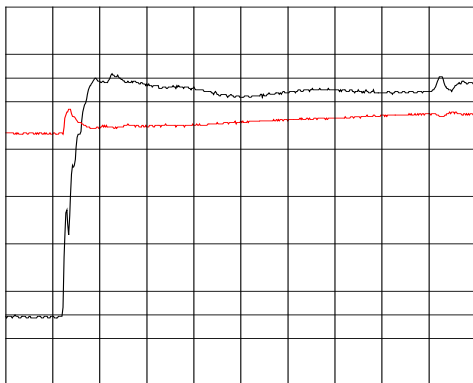

Fig. 14.   Inverter-side line voltage to ground [100V/div.] and line current [10A/div.] time responses [2μs /div.] with complete IRONET.

VI. Conclusions.

The series LNT strategy has been considered for application in medium-to-high power IGBT motor drives.

A novel concept, called IRONET, has been proposed for the exploitation of iron-core power inductors properties as part of wanted LTN high-frequency response. Unwanted high-frequency non idealities have been defined and solutions discussed either analytically or experimentally.

The realization of an IRONET power inductor has been carried-out for 55kW rating by adopting common 0.35 mm thick laminated core, defining   R-C high-frequency compensation of frequency-depending parameters.

The application of proposed IRONET has been experimentally verified, showing how both peak and dangerous high derivative motor voltage values can be actually avoided by cost-effective means, effective also without high-frequency R-C compensation.

The proposed IRONET concept demonstrates how long-life and reliable operation could be achieved for medium-power AC motors by cost-effective efficient solution.
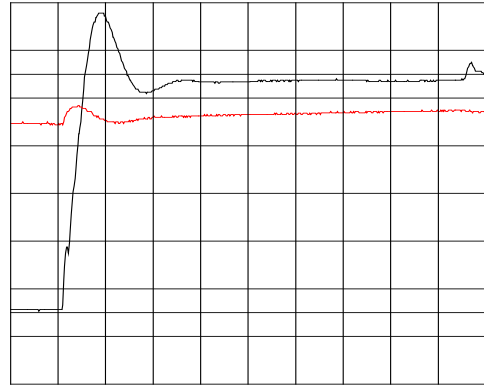

Fig. 15.   Inverter-side line voltage to ground [100V/div.] and line current [10A/div.] time responses [2μs /div.] with IRONET inductor but without R-C compensation.
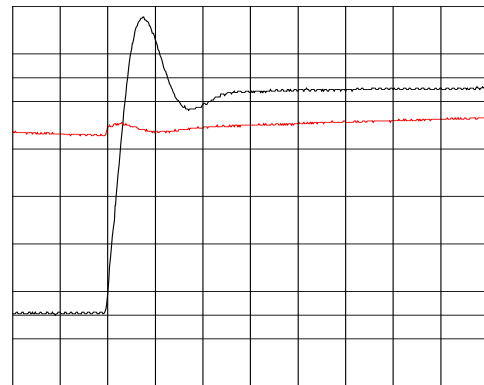

Fig. 16.   Motor voltage to ground [100V/div.] and line current [10A/div.] time responses [2μs /div.] with IRONET inductor but without R-C compensation.

References.

[1] A. Fratta, G.M. Pellegrino, F. Scapino, F. Villata, "A three-phase PWM VSI Line Termination Net for load overvoltage cancellation", Proc. of IEEE ISIE'99, Bled, Slovenia, 12-16 July 1999, pp. 762, 767.
[2] A. Fratta, F. Scapino, F. Villata: "Reflections and Cross-coupling on Three-Phase Cable Connecting PWM-Inverters to the AC-Load", International Conference on Electrical Drives and Power Electronics EDPE'99, High Tatras, Slovak Republic, 5-7 October 1999, pp. 302, 307.
[3] A. Fratta, G.M. Pellegrino, F. Scapino, F. Villata, "Line Termination Net for load overvoltage cancellation in medium to high power three phase PWM VSI Induction Motor drives", Proc. of IEEE ICIT 2000, Goa, India, 19-21 January 2000, pp. 261, 266.
[4] A. Fratta, G.M. Pellegrino, F. Scapino, F. Villata, "Three-phase PWM VSI Induction Motor Drives: VSI power transmission optimization by adopting a series Line Termination ", Proc. of PCIM 2000, Nurnberb, Germany, 6-8 June 2000.
[5] C: Chen, X. XU, "Loss-less & cost-effective terminator topologies with no voltage overshoot", IEEE Applied Power Electronics Conference, APEC '98, pp. 1030, 1034.
[6] S. Ogasawara, H. Ayano, H. Akagi, "Measurement and reduction of EMI radiated by a PWM inverter-fed AC motor drive system", IEEE Transactions on IAS, vol. 33, n. 4, 1997, pp. 1019,1026.
[7] G. Skibinski, "Design methodology of a cable terminator to reduce reflected voltage on AC motor", IEEE IAS Conference Proceedings, 1996, pp. 153, 161.
[8] E. Zhong, T. A. Lipo, S. Rossiter, "Transient modeling and analysis of motor terminal voltage on PWM inverter-fed AC motor drives", IEEE IAS Conference Proceedings, 1998, pp. 773, 780.
[9] S. Bell, J. Sung, "Will Your Motor Insulation Survive a New Adjiustable-Frequency Drive", IEEE Transactions on IAS, vol. 33, n. 5, 1997, pp. 1307, 1311.
[10] A. Carrer, "Note di elettrotecnica", Libreria editrice universitaria Levrotto & Bella, Torino, 1959, chapter XII 12-3.
[11] K. J. Binns, P. J. Lawrenson, C. W. Trowbridge, "Electric and Magnetic Fields", Wiley, Chichester (England), 1992, chapter 4.4.